Available online at www.sciencedirect.com
ScienceDirect
International Journal of Thermal Sciences 47 (2008) 1204–1225
International Journal of Thermal Sciences
www.elsevier.com/locate/ijts

Study on the effect of various parameters on flow development behind vane swirlers

R. Thundil Karuppa Raj, V. Ganesan *

Internal Combustion Engines Laboratory, Department of Mechanical Engineering, Indian Institute of Technology Madras, Chennai 600 036, India

Received 17 October 2006; received in revised form 9 October 2007; accepted 9 October 2007

Available online 3 January 2008

Abstract

Swirl flow has applications in many of the engineering equipments. Good amount of calculations exist which have been developed for design of propellers. However, swirler design for combustion applications is different from that for propeller applications. In the former swirl flow is generated by the application of tangential component to the axial flow whereas in the latter swirl is generated by the rotating propellers. Therefore it comes under the category of rotating flows. Quite a few studies have been carried out on vane generated swirl flows over the past four decades. Majority of the studies were based on experiments. Over the last one decade, attention has been focused on the numerical predictions. Due to the advent of fast digital computers, nowadays the CFD studies are becoming the part of the design methodologies.

This study mainly focuses attention on arriving at best vane angle from aerodynamic aspects for the combustion applications. As there are large number of flow and geometric parameters involved arriving at the best design by experimental methods is rather difficult compared to CFD analyses. The important geometric parameters are vane angle, vane numbers and hub to tip ratio. The flow parameter involves the selection of appropriate turbulence model for the prediction. The uniqueness of this study is in arriving at the best vane angle using appropriate turbulence models for both weak and strong swirl. To this end experimental and numerical studies have been carried out. It is found that no single turbulence model is able to handle both weak and strong swirl. From this study it is concluded that for weak swirl standard k–ε model is sufficient whereas for strong swirl one has to resort to Reynolds stress model. The characteristics of swirl flow are evaluated by means of size of the recirculation zone, mass trapped in the recirculation zone and also the pressure drop. Over the range of vane angle investigated the best vane angle is found to be 45°.

Keywords: Vane swirlers; Recirculation zone; Swirl number; Five hole pitot probe; Vane angle; Hubless swirler; Turbulence models

1. Introduction

Many researchers [1–7] have studied swirling flows in the past since such flows have practical applications in many combustion systems, such as industrial furnaces and gas turbine combustors. Swirling flows in both reacting and non-reacting conditions occur in a wide range of applications such as gas turbines, marine combustors, burners, chemical processing plants, rotary kilns and spray dryers. Swirling jets are used as a means of controlling flames in combustion chambers. The presence of swirl results in setting up of radial and axial pressure gradients, which in turn influence the flow fields. In case of strong swirl the adverse axial pressure gradient is sufficiently large to result in reverse flow along the axis and generating an internal circulation zone. The velocity components and turbulent stresses, which are main characteristics of swirling flows, have been investigated in the past for various configurations to understand the physical process both by experimental investigations and by numerical modeling, complementing each other.

In the present study, the design of vane swirlers is based on the design procedure of Mathur and Macallum [1]. The energy spent in swirl generation and the velocity and static pressure distributions in the jets issuing into the atmosphere are reported with reference to the central recirculation zone. Swirl flows can be characterized by means of a non-dimensional number called the swirl number 'S', which is the ratio of axial flux

* Corresponding author. Tel.: +91 44 22574657; fax: +91 44 22570509, 22574652.
E-mail address: vganesan@iitm.ac.in (V. Ganesan).

1290-0729/$ – see front matter
doi:10.1016/j.ijthermalsci.2007.10.019

Nomenclature

d	hub diameter	mm
D	nozzle exit diameter	mm
M_R	maximum recirculation mass	kg
M_O	mass flow through inlet pipe	kg
R_{ep}	radial distance	mm
S	swirl number	
T_{PLF}	total pressure loss factor	
U_o	average velocity at the inlet	m/s
$U_{r\,\max}$	maximum reverse velocity	m/s
u	time averaged local axial velocity	m/s
v	time averaged local radial velocity	m/s
w	time averaged local tangential or swirl velocity	m/s
X, Y, Z	coordinates	mm

Greek symbols

θ	vane angle	degrees
ϕ	overlap angle	degrees

of swirl momentum (G_Φ) divided by axial flux of axial momentum (G_x) times the equivalent nozzle radius (R). In the present study, swirl number is calculated from $\tan(\theta)$ where θ is the vane angle [2]. The basic characteristic of a weak swirl ($S < 0.3$) is just to increase the width of a free or confined jet flow but not to develop any axial recirculation. This is due to low axial pressure gradient, whereas strong swirl ($S > 0.6$) develops strong axial and radial pressure gradient, which aids to form a central toroidal recirculation zone. The central toroidal recirculation zone (CTRZ) is due to the imbalance between adverse pressure gradient along the jet axis and the kinetic energy of the fluid particles flowing in the axial direction. This is due to dissipation and diffusion of swirl and also by flow divergence [8].

As already mentioned, based on swirl number, the swirl flows are classified into weak, medium and strong swirl. If swirl number is less than 0.3 it is usually classified as weak swirl and if it is between 0.3 and 0.6 it is called medium swirl and if the swirl number is greater than 0.6, it is called strong swirl [9]. The recirculation zone geometry is a direct function of swirl number [3].

In combustors, the central recirculation zone acts as an aerodynamic blockage or a three-dimensional bluff body. This helps in flame stabilization by providing a hot flow of recirculated combustion products and a reduced velocity region where flame speed and flow velocity can be matched. Swirling jets are used in furnaces as a means of controlling the length and stability of the flame. A common method of generating a swirling flow is by employing a vane swirler. This paper focuses on the experimental and numerical study, on the development of recirculation zone behind vane swirlers. Mean velocity measurements have been carried out using a five-hole pitot probe, thus providing a useful database for studying the different factors affecting the formation of recirculation region and turbulent characteristics.

Ganesan [9] has reported by his experimental measurements that the length and width of the recirculation zone increases with an increase in vane angle. In this study a numerical analysis has been carried out to study the effect of hub. For this purpose, flow analysis behind a hubless swirler has been carried out. The effect of hub (with a hub to tip ratio of 0.3) in the formation of recirculation zone and pressure drop has been compared with that of a hubless swirler.

2. Basic geometry and its parts

Swirler geometries with vane angles 15° to 60° in steps of 15° have been created in GAMBIT pre-processor, which are shown in Fig. 1(a). Design details of vane geometry are given for a 45° swirler with 8 vanes of 2 mm thick in Fig. 1(b). The length of the hub is 175 mm and a hemi-spherical nose is attached to the upstream of it to minimize the flow distortion and also to have smooth flow over the hub. Vane angle (θ) indicated in top view is 45° and the overlap angle (ϕ) from the axial direction is 75°. The annular swirl vanes are fixed on the hub of diameter 32 mm and the swirler is fixed in the inlet pipe of diameter 107 mm, which corresponds to a hub to tip ratio of 0.3. The angle subtended by a vane at the axis, when viewed in the axial direction is 75° giving an overlap of 30° between adjacent vanes. The overlap angle is maintained at 30° for 45 and 60 degree swirlers, whereas it is 5° and 0° for 30° and 15° swirlers respectively. It is to be noted that, blade length increases with increase in overlap angle and therefore it is not possible to have 30° overlap for 15° and 30° vane swirlers.

The three dimensional swirler with meshed geometry is shown in Fig. 2. The geometry consists of an inlet pipe of length 500 mm, 107 mm outer diameter and hub diameter of 32 mm. The inlet pipe length of 1500 mm is followed by a square chamber of $250 * 250$ mm cross-section. A tail pipe of 107 mm diameter and length of 1800 mm is provided to avoid the atmospheric disturbances in the development of the flow.

3. Experimental set up and instrumentation

The experiments have been conducted in a sub-sonic, low turbulence wind tunnel. The wind tunnel consists of a blower, a settling chamber with filters and a bell-mouthed nozzle giving a low turbulence level (0.6% at 30 m/s). The three-dimensional swirler geometry is made from transparent acrylic material. The inlet pipe is attached to the wind tunnel as shown in Fig. 3. Holes of 8 mm diameter are drilled downstream of the swirler in the expansion chamber at various stations (A to L) as shown in Fig. 4. A five-hole pitot probe is traversed along these stations (A to L) to obtain the different components of velocities with the help of a 3-D traversing mechanism. It is fully computer controlled and sophisticatedly automated in order to move the probe precisely to the desired location. The traversing mechanism has a provision to rotate the probe mounted on the Z-axis

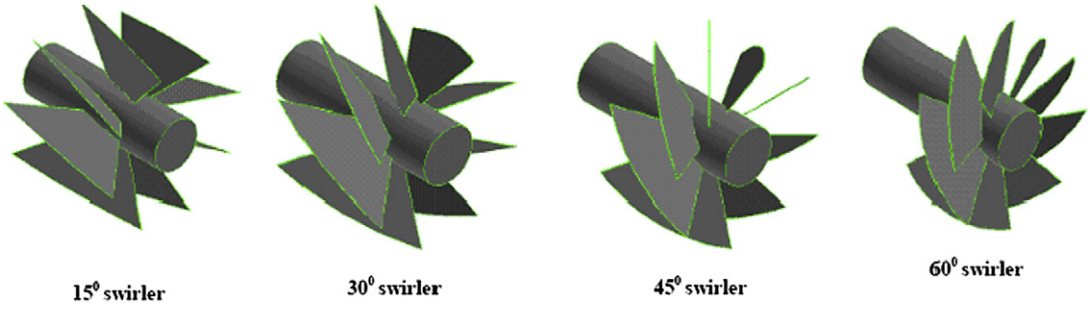

(a)

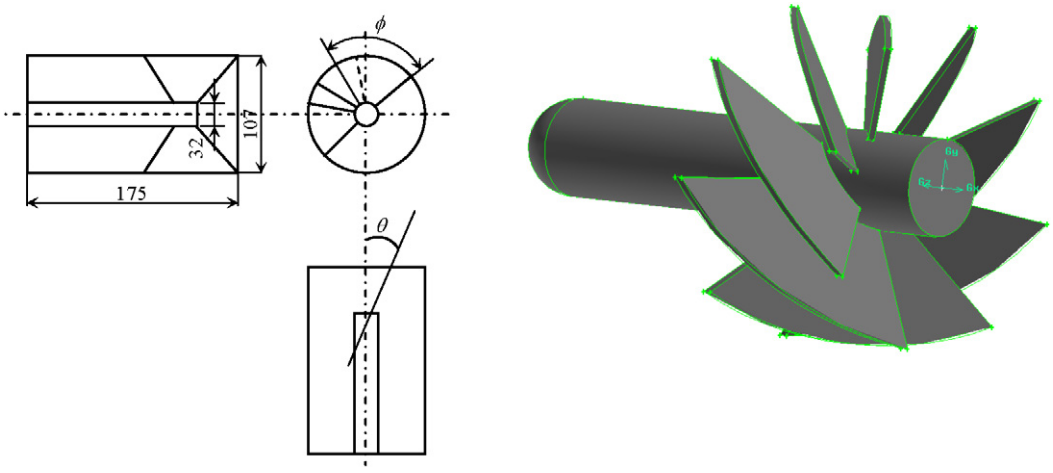

(b)

Fig. 1. (a) Vane swirlers created in gambit pre-processor. (b) Design details of 45° annular vane swirler.

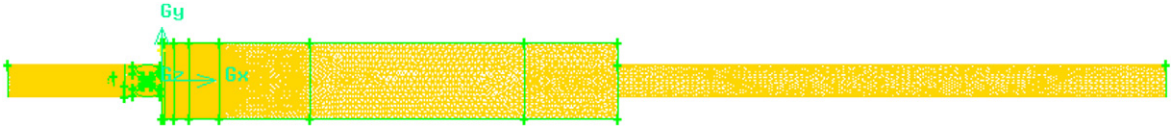

Fig. 2. Meshed geometry under consideration.

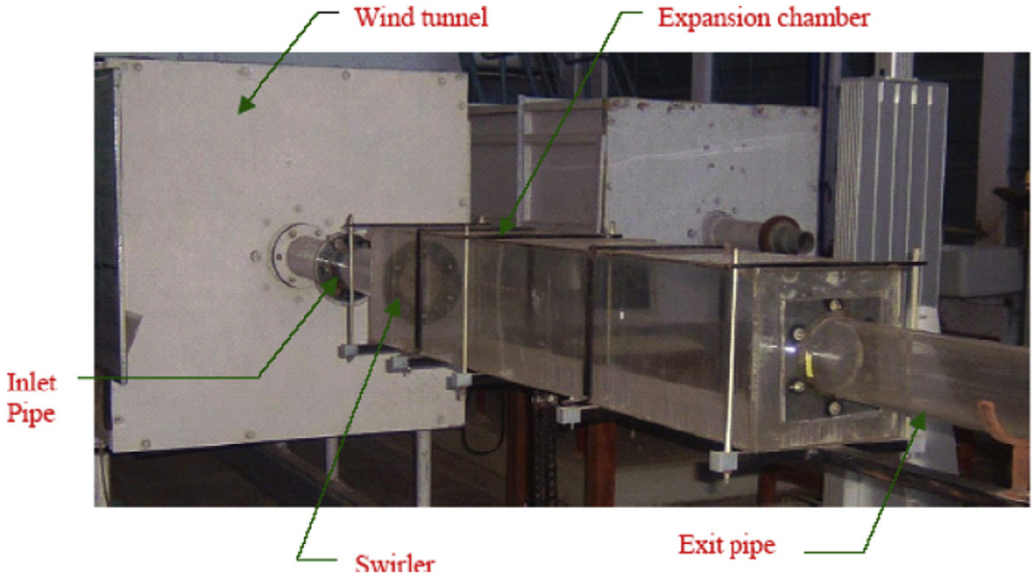

Fig. 3. Photographic view of perspex model of flow through vane swirler.

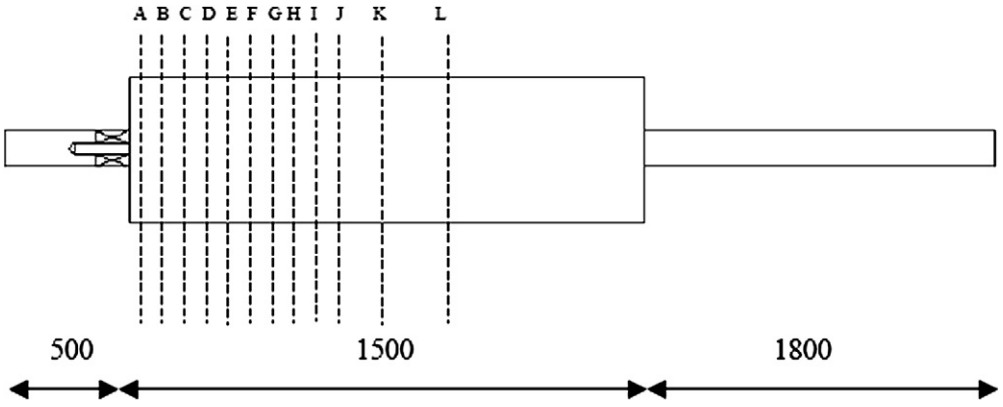

Fig. 4. Details of position of measuring stations indicated by dotted lines (A to L).

having a precision of 1.0 degree, which mainly comes into play when using a five-hole probe during measurement. It has a linear movement accuracy of 1 mm in the entire three axes and a minimum speed accuracy of 0.5 mm/s. It is fully controlled by a computer using the software called "Streamware". Measurements of axial, radial and tangential components of velocities are obtained for every 10 mm radial distance at various X/D axial stations downstream of the swirler. A total of 12 axial locations downstream of the swirler are considered for the measurements.

The instrumentation system consists of five digital micromanometers (Furness controls Ltd., U.K.), whose working range is between -2.5 KPa and $+2.5$ KPa. A minimum pressure of 1 Pascal can be measured. The total working pressure is calibrated along a linear scale of 0 to 10 Volts. The readings in the digital pressure transmitters are recorded directly to the personal computer with the help of 'LABVIEW' software. A user defined program is written so that the average values are obtained over 1000 cycles for each measurement. This is mainly to average the variation in the pressure reading, which shuffles over a range of values.

4. Uncertainty analysis

Chue [10] has shown that five-hole spherical probe can be used in the fixed system over a pitch and yaw range of $\pm 60°$ with an accuracy up to $\pm 0.3\%$ for pitch angle, $\pm 1\%$ for velocity and pressure and $\pm 1\%$ for stream static pressure. Uncertainties associated with the pressure probe measurements are based on data presented by Rhode et al. [11]. The velocity measurements are affected typically by less than 5% for $R_{ep} \geqslant 400$, corresponding to a local velocity greater than 2 m/s, where R_{ep} is the Reynolds number based on probe head diameter. Around 5% error is expected for most of the measurements, increasing up to 10% in regions of low velocity below approximately 2 m/s because of the probe insensitivity to low dynamic pressure.

5. Numerical simulation and turbulence modeling

CFD algorithm used for the present analysis is based on control volume technique. For predicting the flow through the 3-dimensional swirler and through the geometry the following governing equations are solved:

1. Continuity equation and
2. Three momentum equations along the X, Y and Z directions.

A segregated solver is used for solving the above equations. That is, the continuity equation and momentum equations are solved sequentially (segregated from one another). Because the governing equations are non-linear, several iterations in the solution loop are performed to get a converged solution. SIMPLE (Semi-Implicit Pressure Linked Equation) algorithm is applied for solving the above governing equations since the convective terms of the momentum equations contain non-linear quantities. The standard k–ε model of turbulence has been employed to predict the low and medium swirl flows (15° and 30° swirlers) and Reynolds stress model (RSM) is used to predict strong swirl flows as encountered with 45° and 60° swirlers.

The standard k–ε model is a semi-empirical two equation eddy viscosity model, which solves for turbulent kinetic energy (k) and its dissipation rate (ε). The weakness of this model is that it results in excessive turbulence energy in regions where the mean flow is highly accelerated or decelerated. This erroneous prediction of high level of turbulent kinetic energy typically suppresses flow separation and subsequent vortex shedding, if any, downstream of the stagnation point and could not account for prediction of flow with strong streamline curvature as obtained with 45° and 60° vane swirlers. In flows where the turbulence transports or non-equilibrium effects are important, the eddy viscosity model is no longer valid and results of eddy viscosity models are inaccurate. The above problem originates from the way by which the production term is modeled for closure. Hence standard k–ε model of turbulence can predict only low and medium swirl flows.

On the other hand, Reynolds stress model (RSM) of turbulence include the effects of streamline curvature, sudden changes in the strain rate, secondary flows or buoyancy compared to turbulence models using the eddy viscosity approximation. RSM is recommended for free shear flows with strong anisotropy, like strong swirl flows with 45° and 60° vane swirlers. RSM is also recommended for flows with sudden

changes in the mean strain rate, strong streamline curvature and buoyant flows. RSM has superior predictive performance compared to eddy-viscosity models. This is justified, because the RSM solve transport equations for the individual components of the Reynolds stress tensor and the dissipation rate. RSM model is characterized by high degree of universality. The penalty for this flexibility is the high degree of complexity in the resulting numerical calculations. Increased number of transport equations leads to reduced numerical robustness and requires increased computational effort. RSM model not applied to low and medium swirl flows since it could be handled by simple k–ε model.

6. Computational details

The swirler geometry with various vane angle is created in pre-processor GAMBIT. Meshing of swirler vanes is quite complicated especially when there are a large number of vanes with high overlap angle. Unstructured gird has been created using the GAMBIT pre-processor to discretize the computational domain. Due to the presence of large number of vanes and curvature in the vane nearly 1 million tetrahedral cells are used over whole domain (360° sector of the geometry).

The entire geometry is divided into different regions and non-uniform mesh density has been adopted in different regions. A very fine grid density is employed in the region where swirler is placed and also immediate downstream of it (Fig. 2) since a large gradient in flow properties occur in this region. A gradual coursing of the mesh is adopted in the downstream of the swirler. A very coarse mesh is applied to the exit pipe region where not much gradients in flow properties are expected.

Grid independence test has been carried out for all the vane swirlers discussed in the paper. For flow through 45° swirler with 8 vanes geometry, tetrahedral meshing is adopted to overcome the complexity in meshing due to sharp corners and small thickness of vanes. Considering the computational expense and time, the grid with 478 342, 954 969 and 1 773 245 cells for entire 360° sector are used for making grid symmetry analysis. The grid with 954 969 is considered for further analysis since the flow parameter like turbulent kinetic energy at a point near to the exit of the swirler vane is found to be independent even after the mesh size is increased beyond 954 969 cells.

Standard wall function is applied to all the walls, vanes and hub with bluff body. Adiabatic and no-slip boundary conditions are applied at the walls. The meshes near the walls are not much refined to catch the boundary layer growth. This is because, the gradient in flow properties in boundary layer near the wall does not affect the recirculation zone. The pressure loss through swirler strongly depends on the vane angle, the blockage ratio and the type of expansion chamber (either gradual or sudden expansion) and it is independent of near wall flows. Moreover refinement near the walls induces more computational memory and time, with negligible change in pressure loss across the swirler. However, if one wants to go for conjugate heat transfer analysis grid refinements near the wall cannot be ignored. As the present study is on mean flow characteristics such refinements are not undertaken.

The meshed geometry is exported to FLUENT solver for getting the post processing results. To start with the predicted results are validated with the experimental data.

7. Boundary conditions

The boundary conditions used are:

Inlet: The inlet boundary condition involves velocity inlet along with turbulent intensity and hydraulic diameter. The velocity of 20 m/s, turbulence intensity of 1% and hydraulic diameter of 107 mm are specified at inlet.

Outlet: Atmospheric pressure is prescribed at the exit of the domain.

Wall: Wall boundary conditions are enforced on all faces bounding the flow including the vanes and hub with bluff body. Adiabatic, no-slip boundary conditions (i.e. u, v & $w = 0$) are applied at the walls.

Interior: In order to simulate the flow through various volumes that are a part of the entire domain, interior boundary condition is specified at the interface of every two volumes.

Fluid: This boundary condition is applied to all volumes of the geometry for the fluid to flow through. The direction of the flow is along the axial direction.

8. Results and discussion

In the following section, typical experimental results obtained for 15°, 30°, 45° and 60° vane swirler and their predictions using Fluent code are presented and discussed.

8.1. Experimental results

To start with the wind tunnel is calibrated for each swirler, viz. 15°, 30° and 45° vane swirler to give 20 m/s velocity at the inlet. However, the inlet velocity to the 60° swirler could be maintained only at 15 m/s with the available wind tunnel facility since maximum velocity that could be obtained with this swirler is only 15.6 m/s because of excessive blockage to the flow. The decrease in inlet velocity with increasing vane angle is attributed to the increased backpressure developed by the swirler. The calibration of wind tunnel is done by measuring wall static pressure and the dynamic pressure at the inlet pipe with the help of a differential pressure transmitter and pitot static tube respectively.

8.1.1. Fifteen degree annular vane swirler

Figs. 5 and 6 represent the mean axial velocity profiles obtained for 15° annular vane swirler. The experimental readings are taken along one side considering the symmetry of the geometry about the axis. The velocities are normalized with respect to incoming velocity (U_0) of 20 m/s. Taking into account the uncertainties in measurements, the agreement between the numerical results and the experiments can be termed as good in almost all stations (Fig. 5). The maximum deviation between the predicted and measured data is less than 5% at most of the

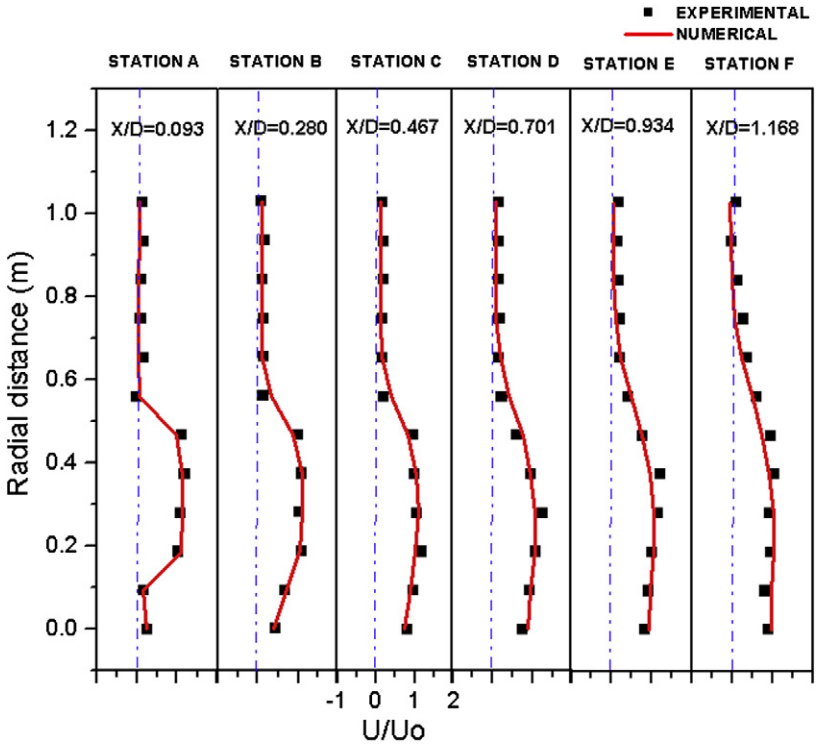

Fig. 5. Comparison of axial velocity profile of 15° swirler (A to F).

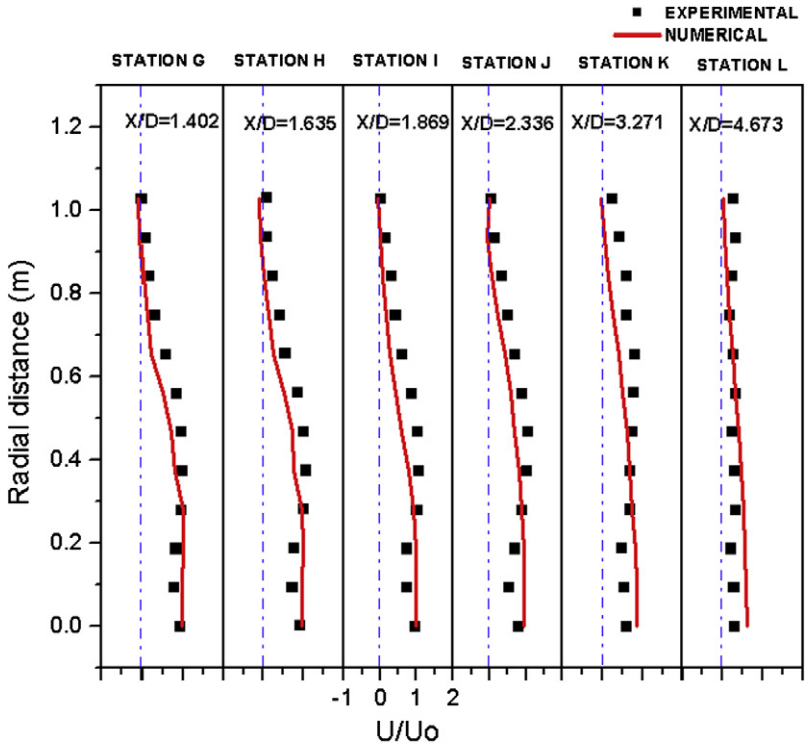

Fig. 6. Comparison of axial velocity profile of 15° swirler (G to L).

stations where velocity is greater than 2 m/s and is of the order of 10 to 15% when the velocity is less than 2 m/s. It is to be expected that five-hole probe is not very sensitive at low velocities. It can be noted from the Figs. 5 and 6, that there is no negative velocity in any of the stations (A to L). This indicates that 15° swirler is not able to develop any central recirculation zone since swirl is weak in nature. The flow emerges as multiple jets between the vanes. The change in the velocity is almost negligible beyond $X/D = 4.67$ and the velocity profiles are self-similar.

At station 'A' the velocity distribution show a wake profile due to hub effect. As can be seen in first six stations (A to F), the

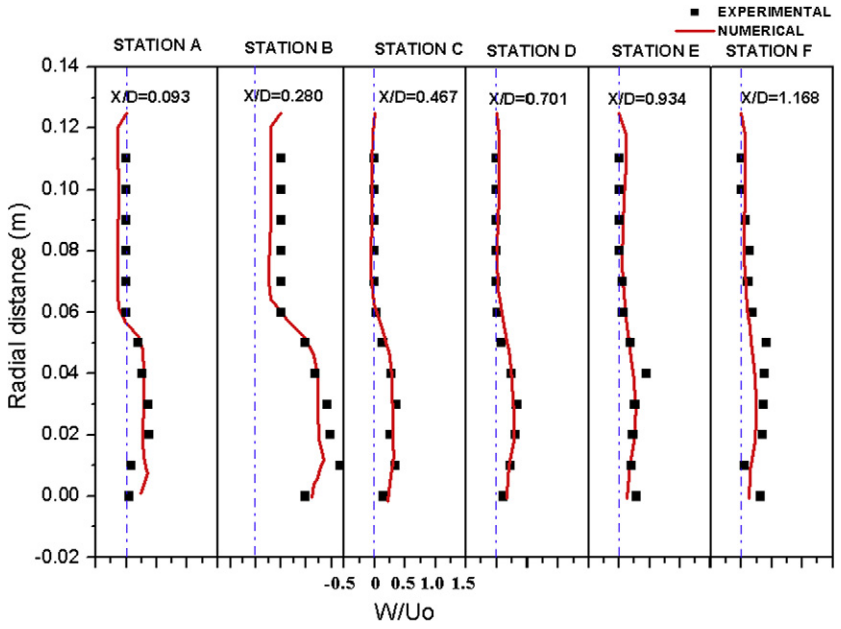

Fig. 7. Tangential velocity profile of 15° swirler (A to F).

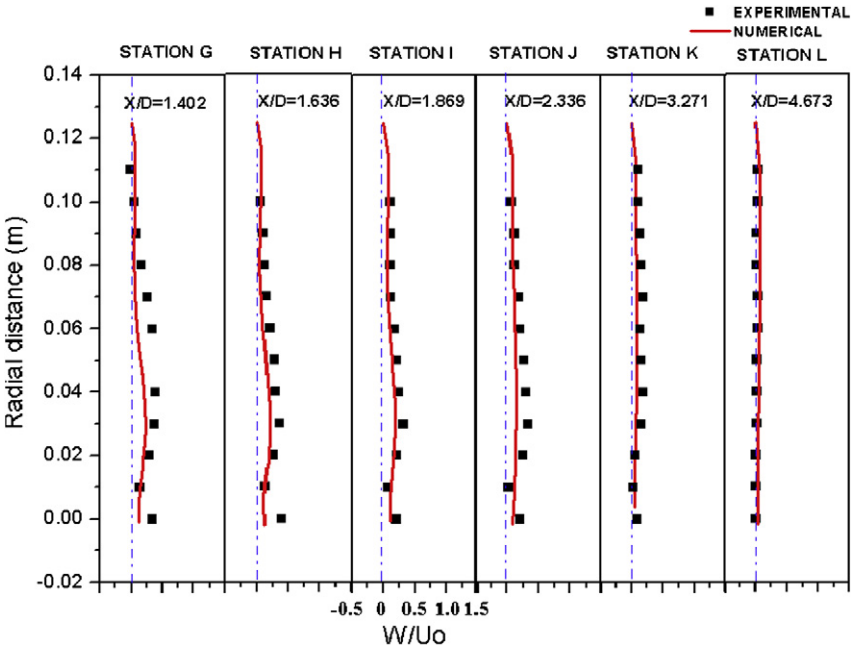

Fig. 8. Tangential velocity profile of 15° swirler (G to L).

numerical results predicted with standard k–ε model matches quite well and predict the overall swirl flow field reasonably well. For the last six stations (G to L), the predictions can be said to be reasonably good except at stations K and L. In these stations there is some deviation, which may be attributed to the fact the flow becomes fully developed turbulent flow and measurements in these stations are rather difficult. Further, the far downstream flow field is not going to affect swirl flow field development close to the swirler.

The radial velocity seems to have littler influence on the swirl flow field. This is because, the strength of the swirl flow is defined by a non-dimensional number 'S' which is the ratio of axial flux of tangential momentum to the axial flux of axial momentum times the nozzle radius 'R'. Thus, the strength of the swirl flow is much influenced by tangential and axial velocity components as compared to radial velocity component.

Figs. 7 and 8 show the tangential velocity profiles for 15° vane swirler for the stations 'A' to 'F' and 'G' to 'L' respectively. The tangential velocity component greatly influences the swirl flow as the strength of the swirl flow directly depends on the tangential velocity component. It is seen from Figs. 7 and 8 that the matching of numerical results with that of experiments is good except at some points in stations 'F' and 'G' where

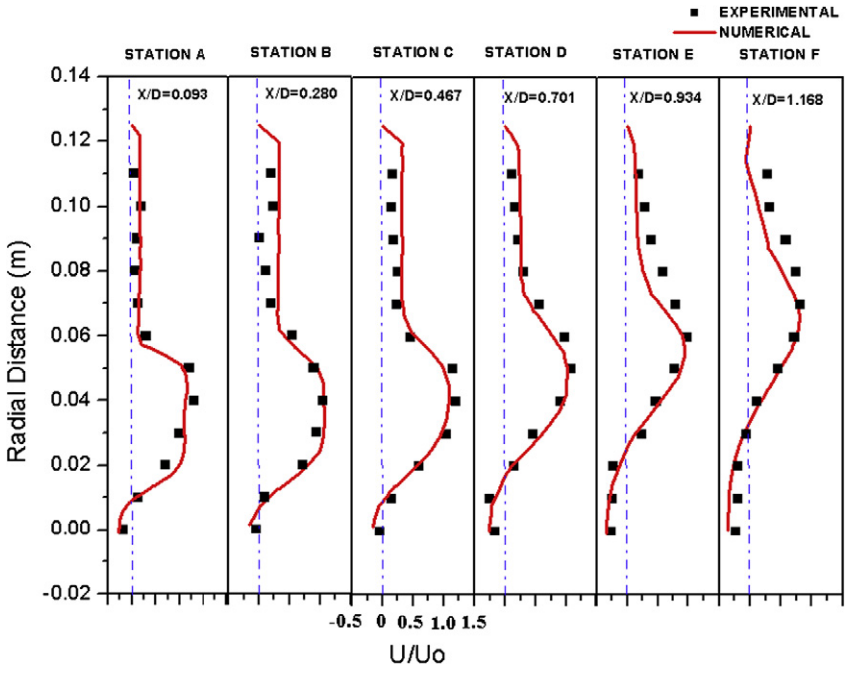

Fig. 9. Axial velocity profile of 30° swirler (A to F).

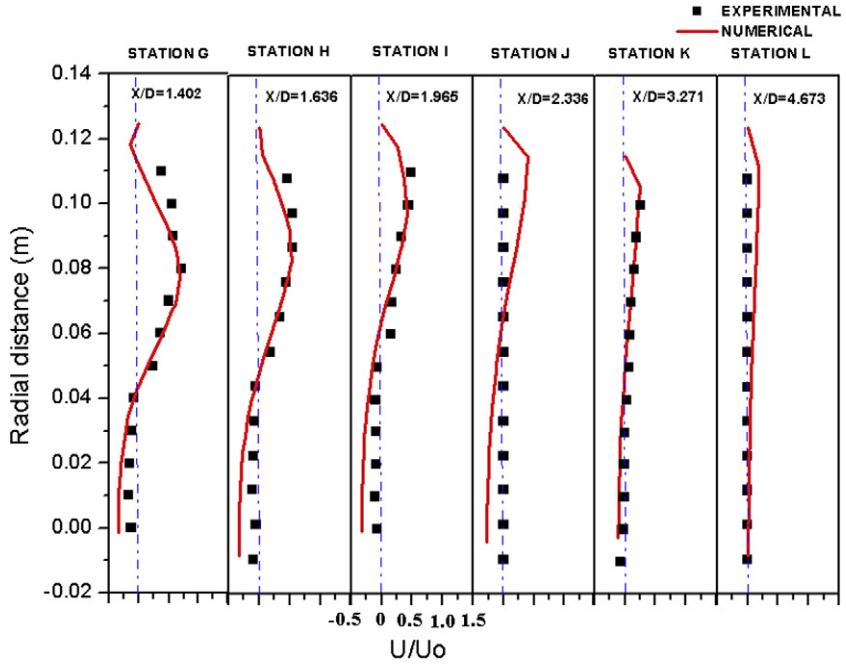

Fig. 10. Axial velocity profile of 30° swirler (G to L).

there exists a slight deviation between the two. It is found that the tangential velocity is maximum in the core region and decays as the flow proceed downstream of the swirler indicating the decay of swirl. The tangential velocity reaches almost zero at the axial location 'L' which indicates that the flow has lost its swirling characteristics.

8.1.2. Thirty degree annular vane swirler

Figs. 9 and 10 show the axial velocity profile obtained for a 30° vane swirler. It is seen that the matching of the numerical results with that of the experiment is reasonably good in almost all the planes. It is seen from Figs. 9 and 10 that the axial velocity values show a peak, where the flow comes out, through the vanes. This is due to the kinetic energy increase as it passes between the vanes which acts as nozzle. The magnitude of the axial velocity gradually decreases from station 'A' to 'F'. However, the peak shifts towards outer wall indicating the expansion of jet. Further, that there exists a small region of negative velocity indicating recirculation very close to the axis at station 'A'. This recirculation zone gradually expands as the flow proceeds

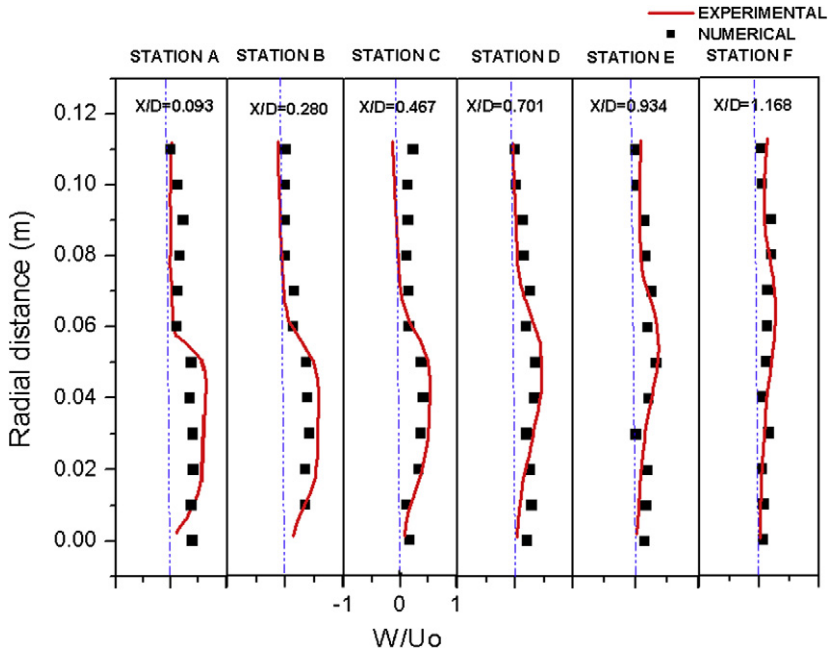

Fig. 11. Tangential velocity profile of 30° swirler (A to F).

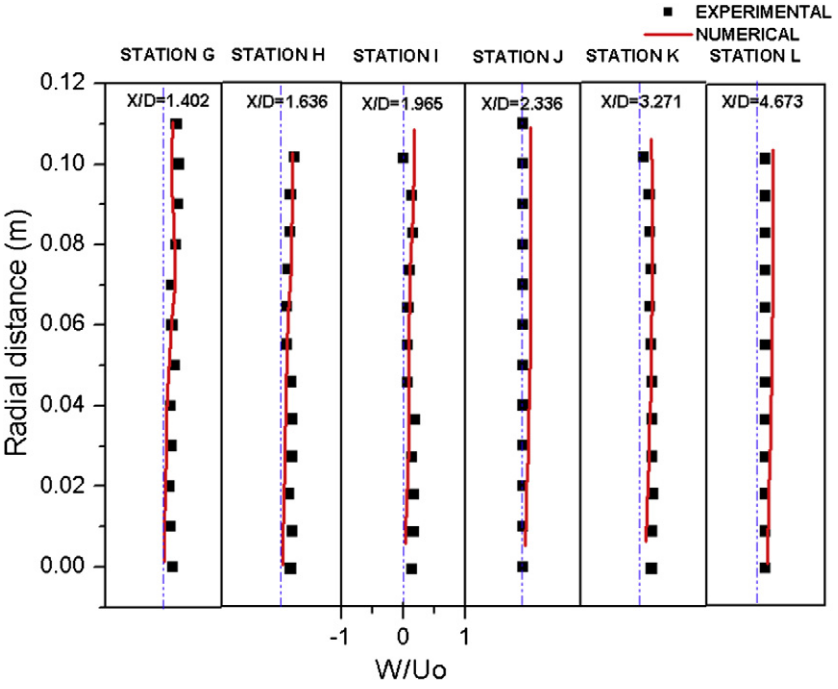

Fig. 12. Tangential velocity profile of 30° swirler (G to L).

axially downstream of the swirler and it extend to a maximum width of 50 mm on either side of the axis at axial plane 'H' thereafter starts decreasing. The recirculation zone almost vanishes after plane 'K' and thereafter the flow becomes more or less uniform.

Figs. 11 and 12 show the tangential velocity obtained for 30° vane swirler. The matching of the numerical results with that of the experiment is quite reasonable from station 'C' to 'L' and some deviation is found in the first two stations namely 'A' and 'B'. The above discrepancies are due to the fact that during the measurements the five hole pitot probe could not be made to null accurately close to the swirler hub due to large flow fluctuations at these stations. However, the trend is very well predicted. The tangential velocity component increases radially from the centre to the wall as it proceeds axially from plane 'A' to 'G'. It is seen that there exists a small central recirculation zone in case of 30° vane swirler, which is not seen in case of 15° swirler. Hence from this analysis, even for the 30° swirler it can be seen that standard k–ε is able to predict the weak swirl reasonably well.

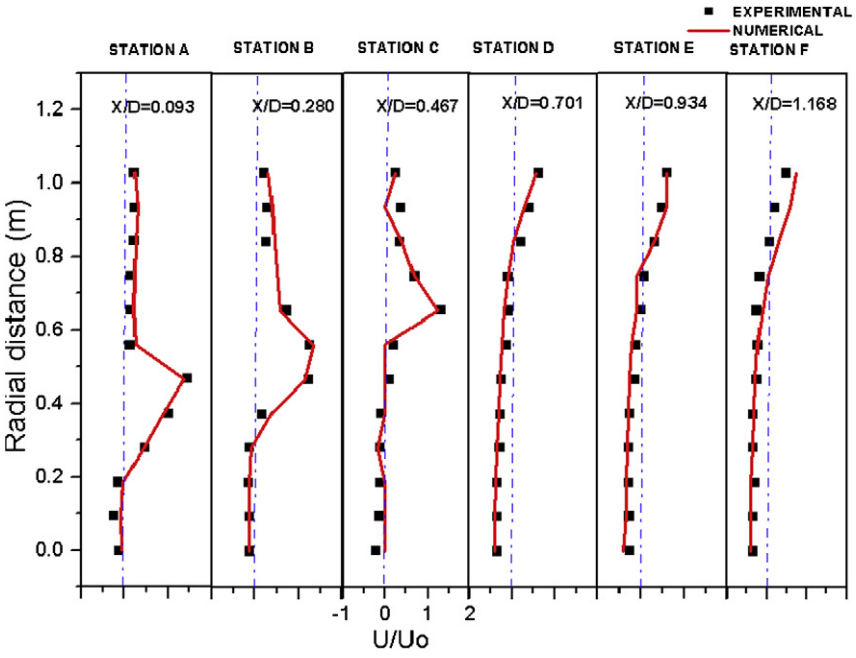

Fig. 13. Axial velocity profile of 45° swirler (A to F).

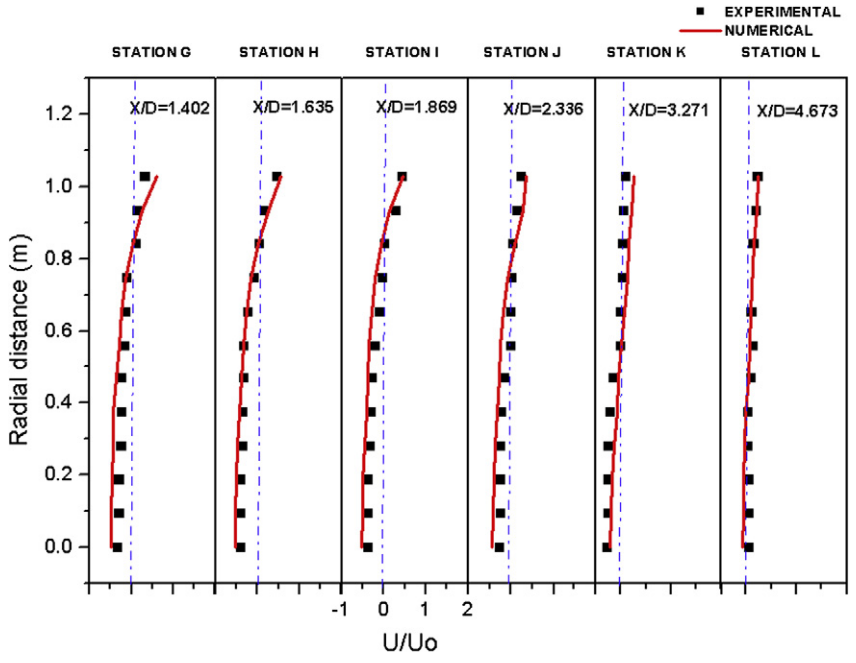

Fig. 14. Axial velocity profile of 45° swirler (G to L).

8.1.3. Forty five degree annular vane swirler

Figs. 13 and 14 show the axial velocity profile of a 45° vane swirler. The predictions are made using Reynolds stress model (RSM) as k–ε model was not able to handle the flow. It is found that the axial velocity predicted numerically with RSM matches well with the experiment in almost all the stations from axial plane 'A' to 'L'. A small discrepancy is seen at some radial positions in planes 'A' to 'C'. Here also the experimental reading taken with the help of five-hole pitot sphere experienced some difficulty in measuring the velocity behind the hub region. It is seen that there exists negative velocity starting from plane 'A' itself extending 20 mm radially on either side of the central axis. The recirculation zone extends rapidly on either side of the central axis as the flow proceeds downstream of the swirler. The recirculation width is maximum at planes F to I extending to 100 mm on either side radially on the central axis.

Figs. 15 and 16 show the tangential velocity profiles obtained for 45° vane swirler. The agreement between the numerical results and experiment is quite reasonable at all the planes. As expected the tangential velocity value is maximum at plane 'A' and starts decreasing as moving further downstream. The tangential velocity at planes 'G' to 'L' is almost constant.

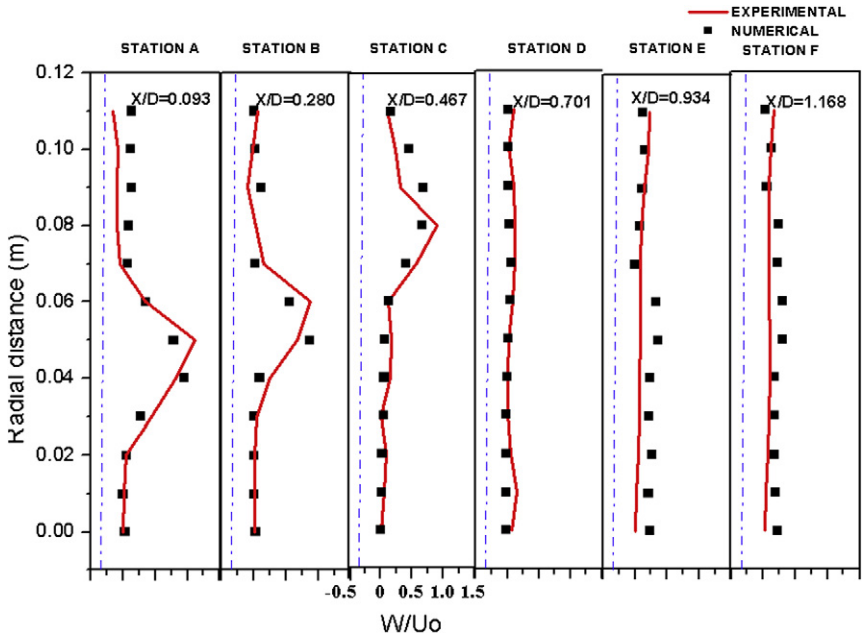

Fig. 15. Tangential velocity profile of 45° swirler (A to F).

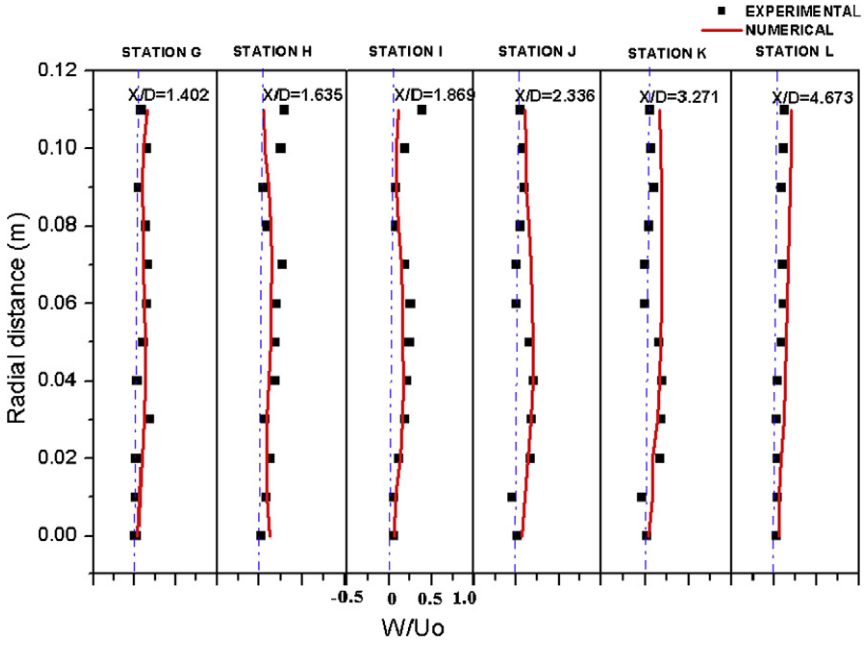

Fig. 16. Tangential velocity profile of 45° swirler (G to L).

Thus the Reynolds stress model (RSM) of turbulence is able to predict well the experimental results for strong swirls as encountered with 45° vane swirler.

8.1.4. Sixty degree annular vane swirler

Figs. 17 and 18 show the axial velocity profile obtained for a 60° vane swirler. A reasonably good agreement exists between the numerical results and the experimental values. The profiles show positive values at some radial points in two planes namely 'A' and 'B' whereas negative velocity is seen at all radial points in all the axial locations except near the walls. The predicted results even show a very small negative velocity at the axial plane 'L'. The profile shows a good central recirculation zone through out the entire axial plane locations. The width of the central recirculation zone extends up to 100 mm on either side of the central axis. The size and shape of the central recirculation zone is larger than that of the 45° vane swirler.

Figs. 19 and 20 shows the tangential velocity profile obtained for a 60° vane swirler. A reasonable agreement between the predicted values with the experimental data is obtained at axial locations from 'D' to 'L'. Small discrepancies in tangential velocity is seen at some radial locations in axial planes namely 'A' to 'C'. The radial velocity, which is very small and negligible as compared to the axial and tangen-

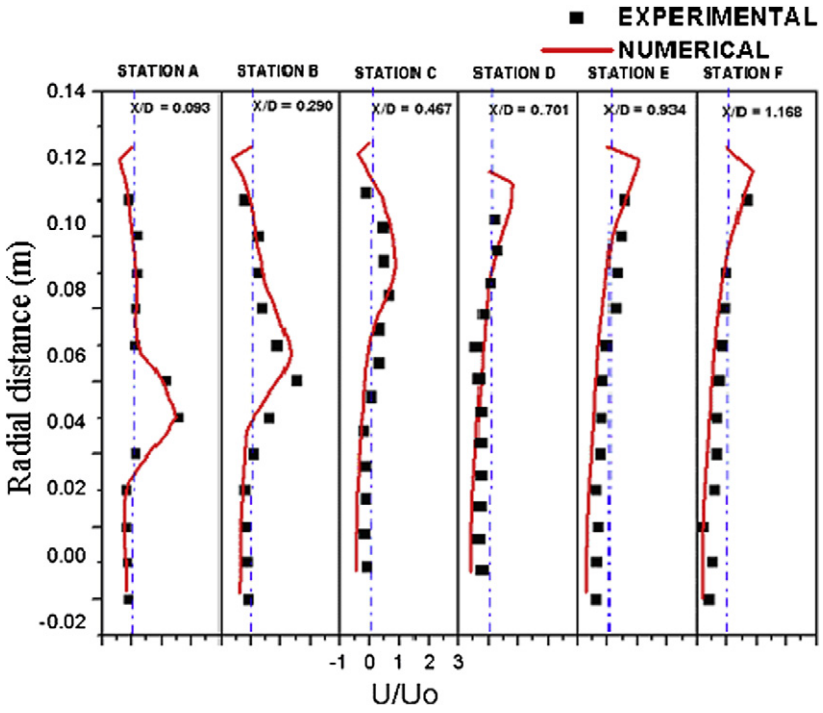

Fig. 17. Axial velocity profile of 60° swirler (A to F).

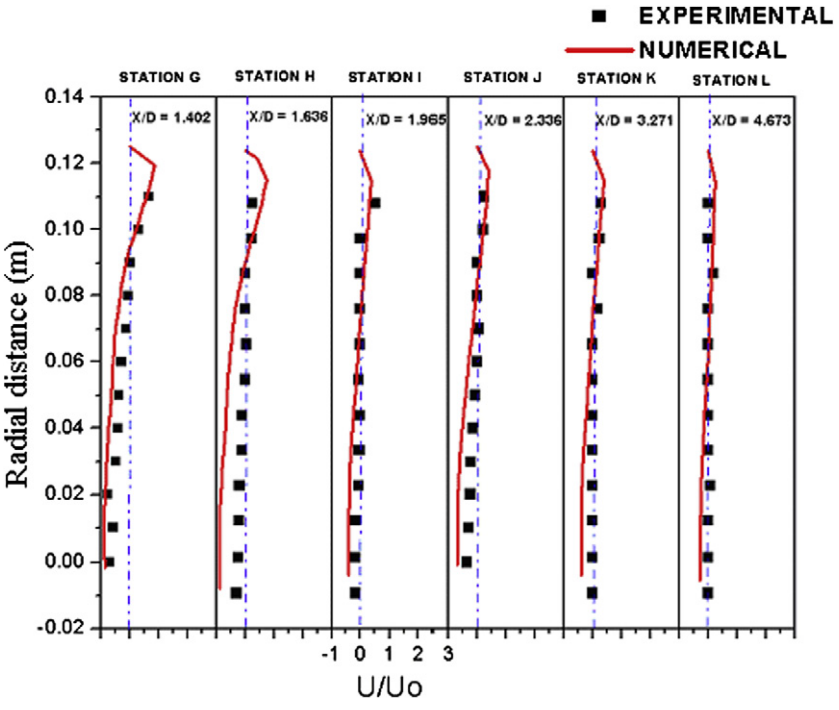

Fig. 18. Axial velocity profile of 60° swirler (G to L).

tial velocity, is not presented here. Thus the Reynolds stress model of turbulence is able to predict the strong swirl flow for 60° vane swirler also. The numerical validation of axial and tangential velocity profiles with experiment is quite reasonable over the first eight stations (i.e. from A to H) extending from swirler exit to 175 mm downstream, where the effective recirculation zone exists for all the swirlers investigated. A slight difference is found between the prediction and experiments further downstream, where the velocity magnitude is quite low.

Based on the above validation, it is proposed to conduct following parametric studies on flow through vane swirlers.

(i) Effect of vane angle;
(ii) Effect of number of vanes; and
(iii) Hub effect.

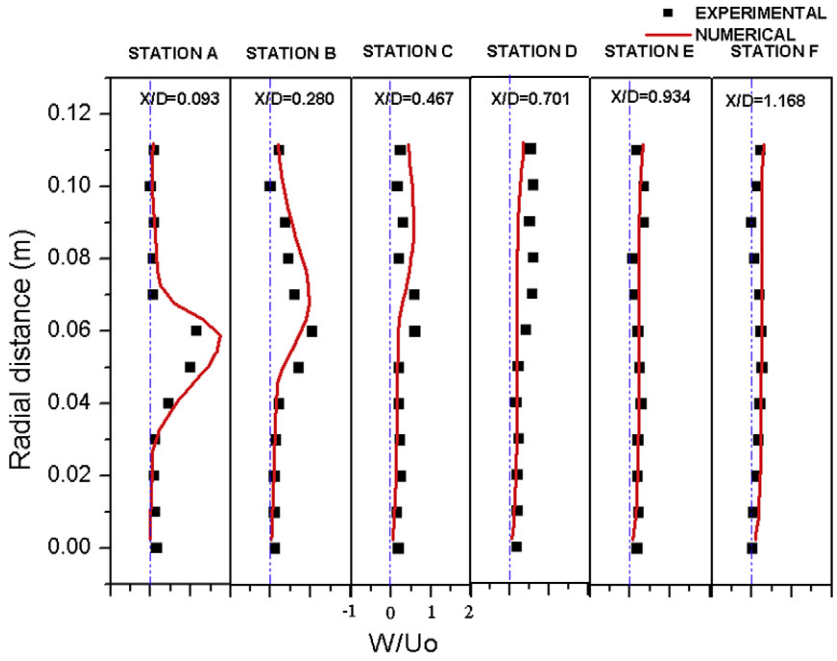

Fig. 19. Tangential velocity profile of 60° swirler (A to F).

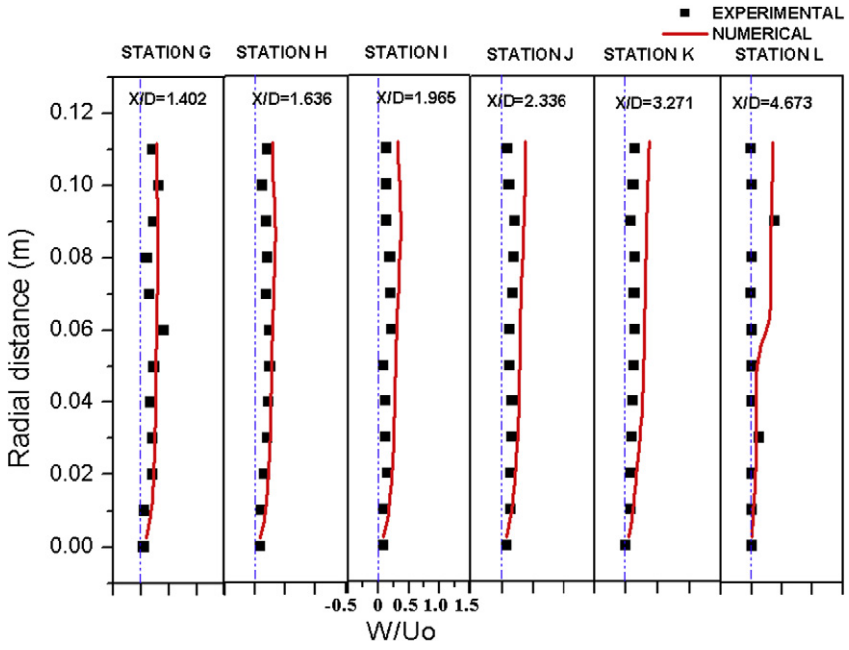

Fig. 20. Tangential velocity profile of 60° swirler (G to L).

8.2. *Effect of vane angle on swirl flow field characteristics*

In swirling flows vane angle exerts a significant effect on the flow characteristics. In this section the effect of vane angle on the flow development is presented and discussed.

8.2.1. *Axial velocity and recirculation zone*

The axial velocity distribution in the mid plane for 15°, 30°, 45° and 60° vane swirlers are shown in Figs. 21 to 24 respectively. It is seen from Fig. 21 that the velocity magnitude in the central zone has only positive values. It is found that in case of 15° swirler only the hub effect predominates and development of recirculation bubble is only very close to the hub.

The flow downstream of 30° swirler shows maximum reverse velocity of 7.11 m/s as seen from Fig. 22, which shows the formation of recirculation zone. Maximum reverse velocity magnitude of 10.4 and 14.3 m/s are found for 45° and 60° swirlers respectively as seen from Figs. 23 and 24. Figs. 25–27 and 31–33 show velocity contours within the recirculation zone for various vane swirlers. These contours are obtained by plotting the axial velocities which ranges from zero to maximum negative value within the recirculation zone. The recirculation

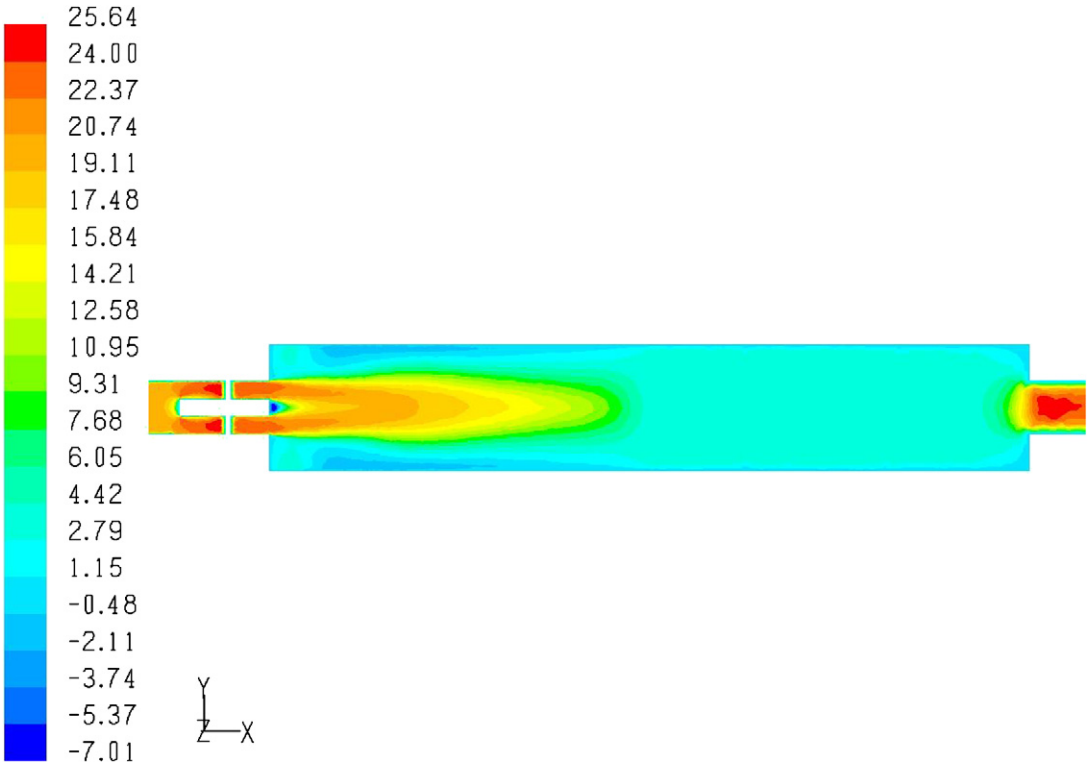

Fig. 21. Axial velocity contour in mid-plane for 15° swirler.

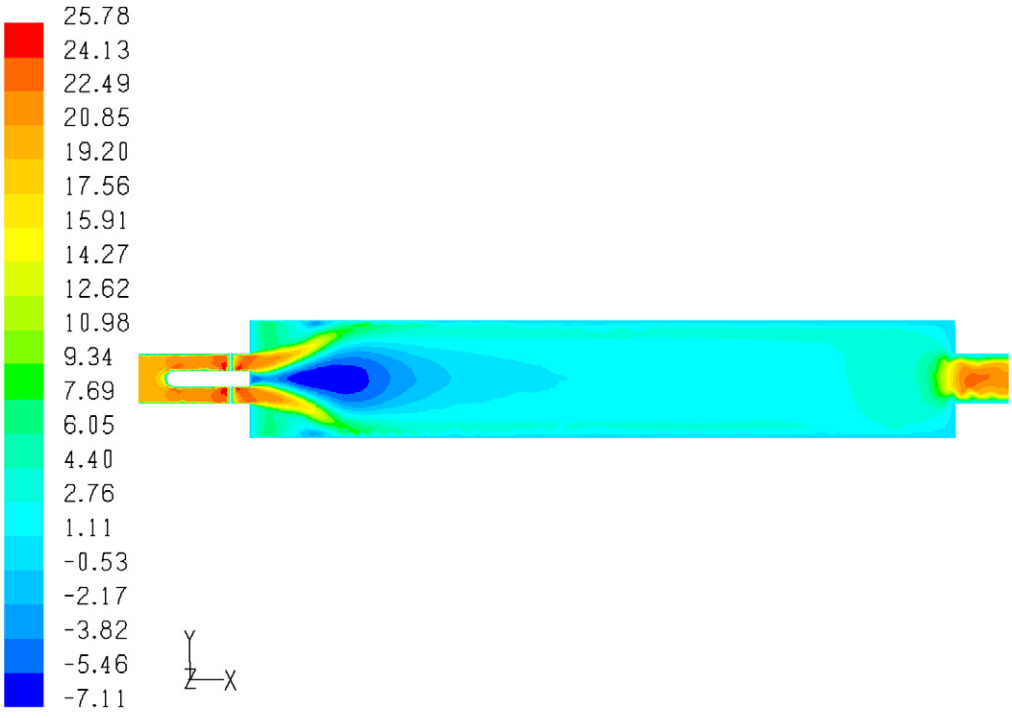

Fig. 22. Axial velocity contour in mid-plane for 30° swirler.

zone in the mid plane downstream for the 30° swirler is shown in Fig. 25. The region with reverse velocity is termed as central re-circulation zone, which is mainly responsible for flame stabilization. As can be seen from Fig. 25 that the recirculation zone is narrow and short having a width of 1.33 D and length 4.44 D where 'D' is the swirler diameter. This recirculation zone is critical as far as the residence time for the reactant species and the heat transfer rate are concerned. The above parameters in turn depend on the volume and surface area (S_A) of the recirculation zone. Hence it will be useful to investigate the effect of the vane angle on the geometry namely the length, width, surface area and the volume of the recirculation zone.

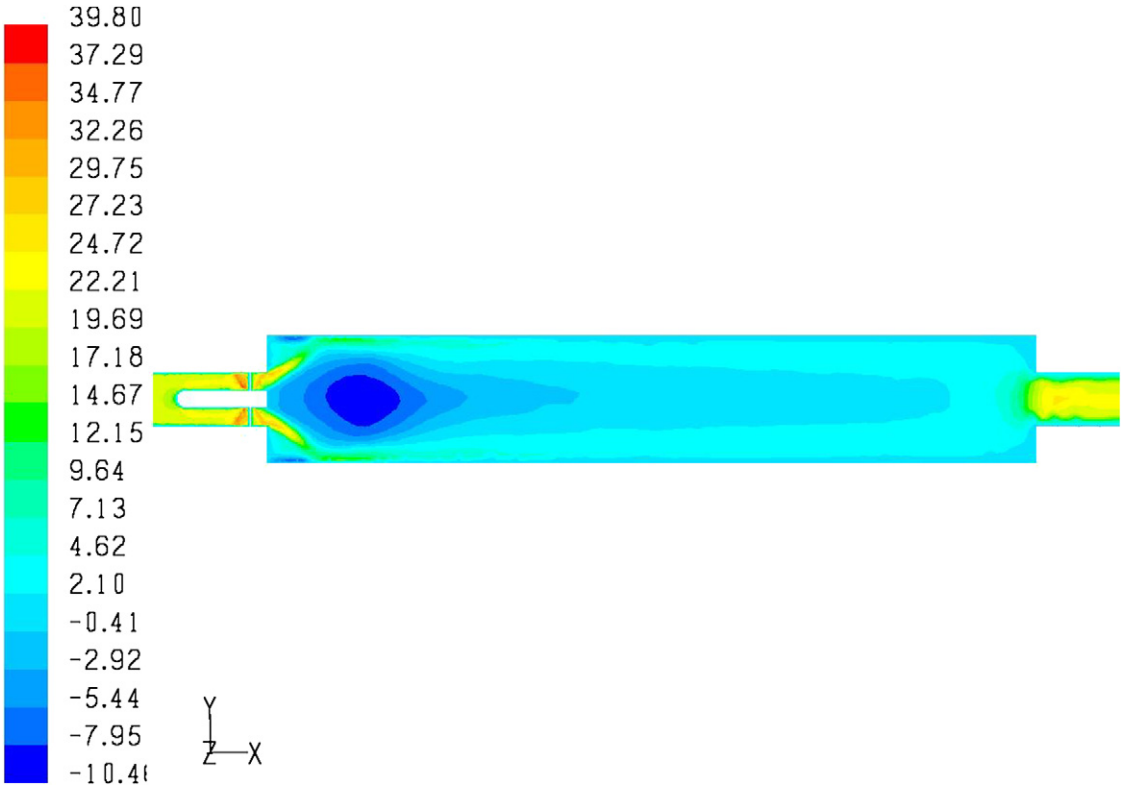

Fig. 23. Axial velocity contour in mid-plane for 45° swirler.

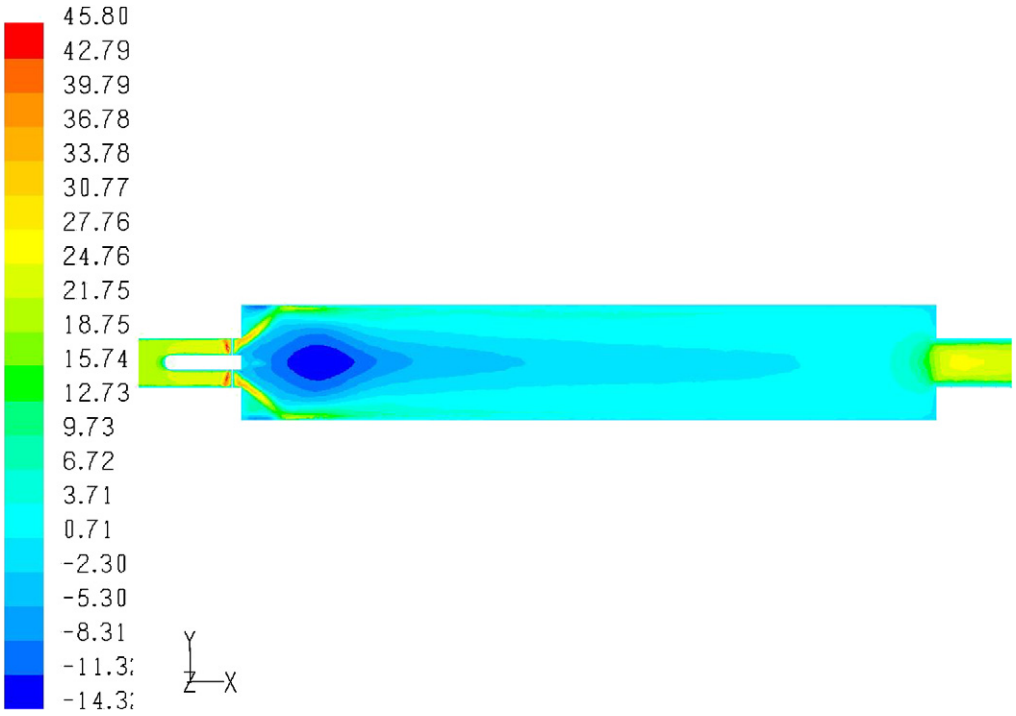

Fig. 24. Axial velocity contour in mid-plane for 60° swirler.

For the 45° vane swirler, it is seen from Fig. 26 that the width of the re-circulation zone has increased compared to 30° swirler, and the largest width is obtained for the 60° swirl angle as can be seen from Fig. 27. The characteristics of the recirculating zone like the size (length and width to diameter ratio), the surface to volume ratio, the rate of maximum recirculating mass to the inlet mass (M_R/M_O), the pressure loss factor (PLF) of various swirlers are given in Table 1. As already reported by Ganesan (1974), this study also illustrate that the length and width of the recirculation zone increases with increase in vane

angle. Thus it is seen that the vane angle has a predominant effect on the central recirculation zone. In case of 60° swirler it is found that the length of the recirculation zone is longer than 45 degree swirler.

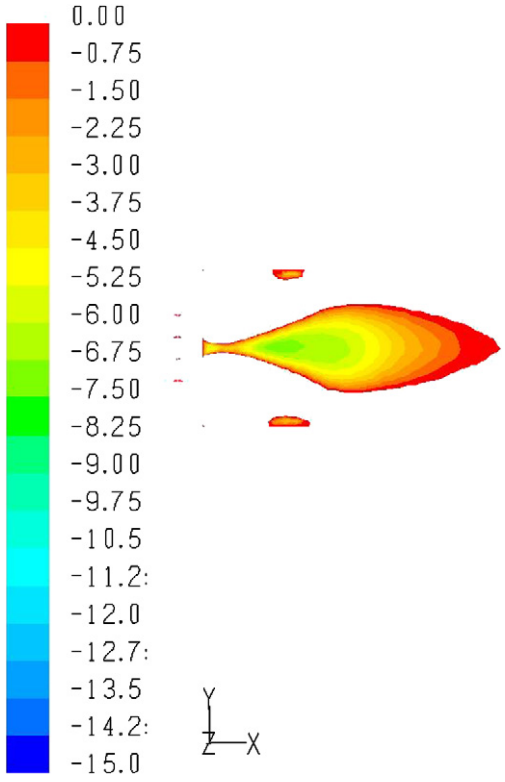

Fig. 25. Velocity contour within recirculation zone for 30° swirler.

8.2.2. Recirculation mass, reverse velocity and Pressure Loss Factor (PLF)

The recirculation mass is defined as the mass of particles present downstream of the swirler with reverse (negative) velocity. It is the product of density, maximum reverse velocity and cross-sectional area at which maximum reverse velocity oc-

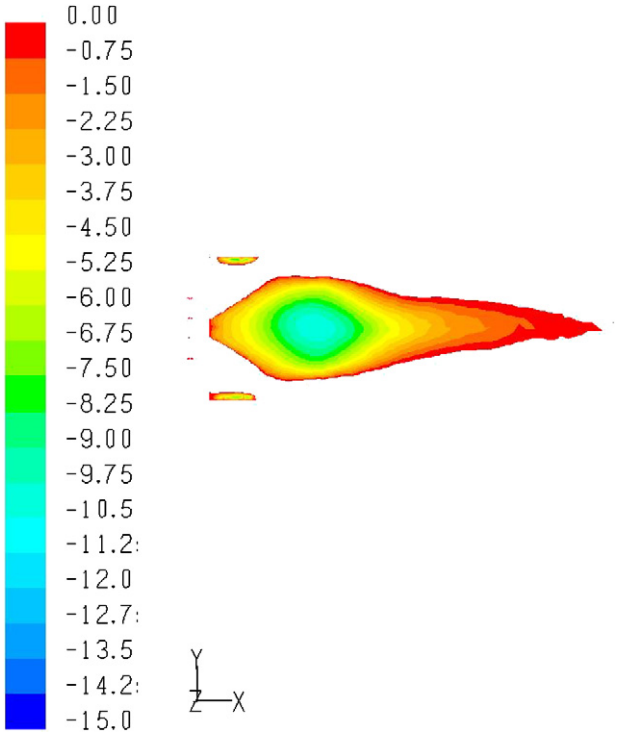

Fig. 26. Velocity contour within recirculation zone for 45° swirler.

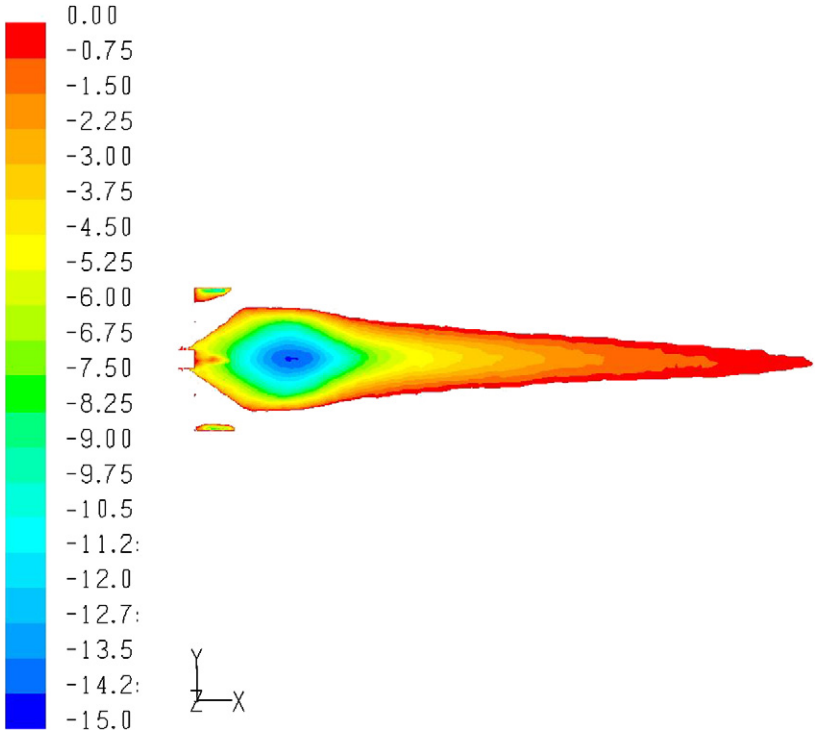

Fig. 27. Velocity contour within recirculation zone for 60° swirler.

Table 1
Characteristics and dimensions of recirculation zone for various swirlers

S. No	Vane angle	S	L/D	W/D	$U_{r\,\max}/U_o$	PLF	M_R/M_O	S_A/V (per unit)
1	15°	0.27	–	–	0.00	0.74	–	–
2	30°	0.57	4.44	1.33	0.35	2.80	0.18	0.040
3	45°	1.00	6.54	1.70	0.53	5.65	0.74	0.030
4	60°	1.73	10.28	1.76	0.77	15.4	0.96	0.031

$U_{r\,\max}$ refers maximum reverse velocity and U_o refers average inlet velocity.

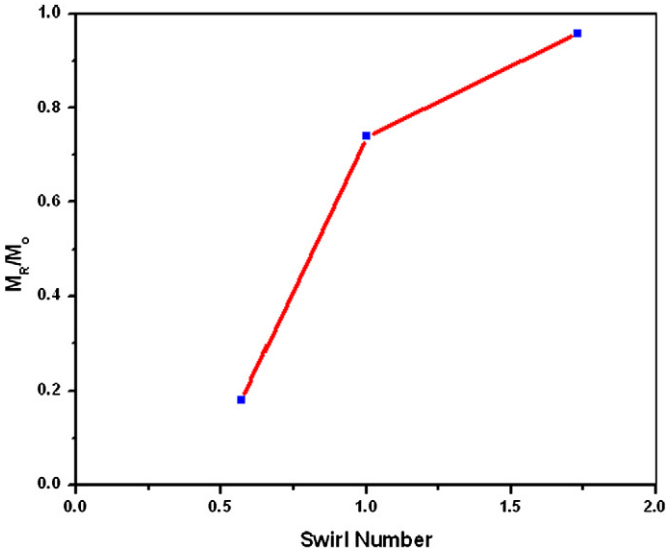

Fig. 28. Maximum recirculation mass of various swirlers.

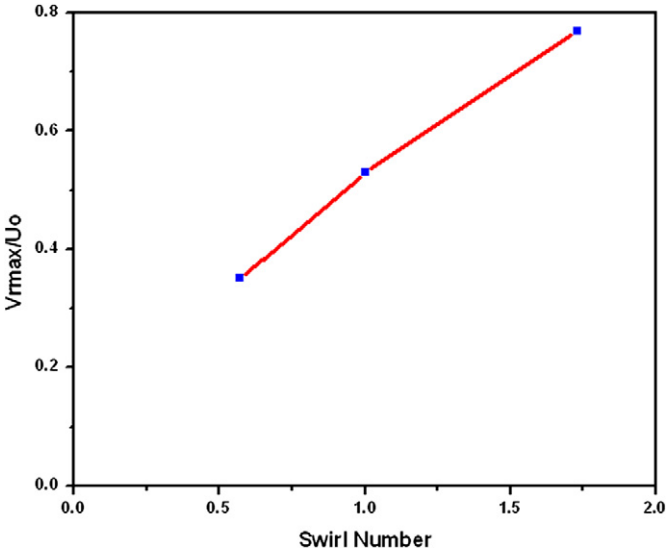

Fig. 29. Maximum reverse velocity of various swirlers.

curs. A graph showing the relation between maximum reverse mass to nozzle mass and vane angle for various swirlers are shown in Fig. 28. It is seen that the larger reverse mass flow is seen for 60° swirler. The ratio of the maximum reverse flow to the nozzle flow for various swirlers is shown in Fig. 29. It is seen that both maximum recirculation mass and maximum reverse velocity increases with increase in vane angle.

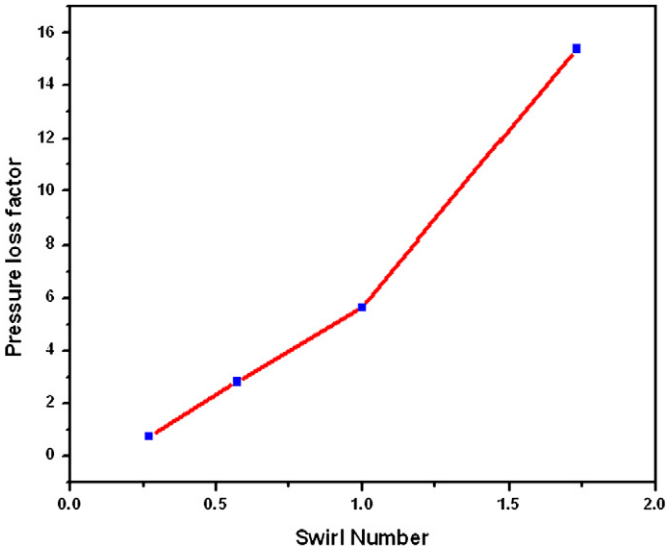

Fig. 30. Total pressure loss factor of various swirlers.

Total Pressure loss factor (PLF) is a dimensionless number and is defined as

$$\text{Pressure Loss Factor (PLF)} = \frac{P_{02} - P_{01}}{\frac{1}{2}\rho U_o^2}$$

where the inlet stagnation pressure (P_{01}) is measured in the inlet pipe upstream of the swirler and exit stagnation pressure (P_{02}) is obtained in the tail end pipe leaving to the atmosphere, ρ is density of the fluid in kg/m^3 and U_o is mean bulk inlet velocity to swirler (m/s).

The variation of pressure loss factor is shown in Fig. 30 and it is seen that with increase in vane angle pressure loss factor also increases. As can be seen from the figure that there is a very steep increase when the vane angle is increased from 45° to 60°.

For efficient design of combustion chamber the pressure loss factor should be as minimum as possible but at the same time it should have more recirculation mass in the recirculation zone. So a compromise is needed between the recirculation zone formed and the total pressure loss across the swirler. Taking these factors into account it is found that the total pressure loss factor across 60° swirler is nearly 3 times higher than that for 45° swirler as well the recirculation zone size of both the 45° and 60° are almost the same.

To summarize, the effect of vane angle, the characteristics and dimensions of the recirculation zone for various vane swirlers are given in Table 1. It is seen that no recirculation zone is formed with 15° swirler and larger and larger recirculation zones are formed for 45° and 60° degree swirlers respectively. The maximum reverse mass to nozzle mass (M_R/M_O) increases as vane angle increases. The surface area to volume ratio (S_A/V) of recirculation zone formed for 45° and 60° swirlers are almost the same but the pressure loss factor (PLF) for 60° swirler is approximately thrice that of the 45° swirler. Hence it is concluded that the 45° vane swirler produces good recirculation zone with reasonable pressure drop, which may aid better combustion.

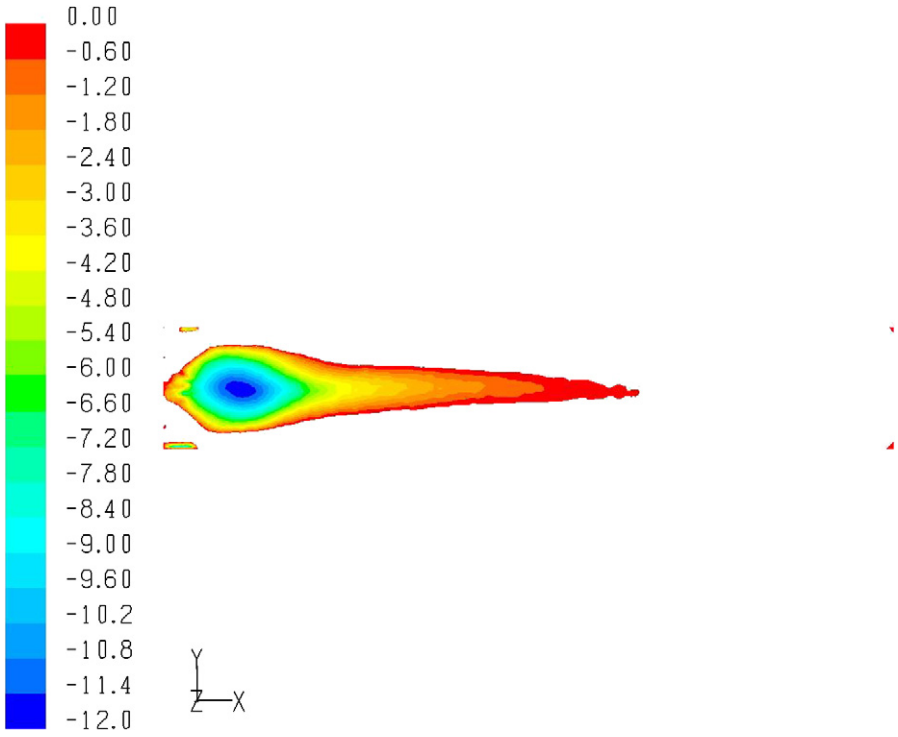

Fig. 31. Velocity contour within the recirculation zone for 4 blades of 45° swirler.

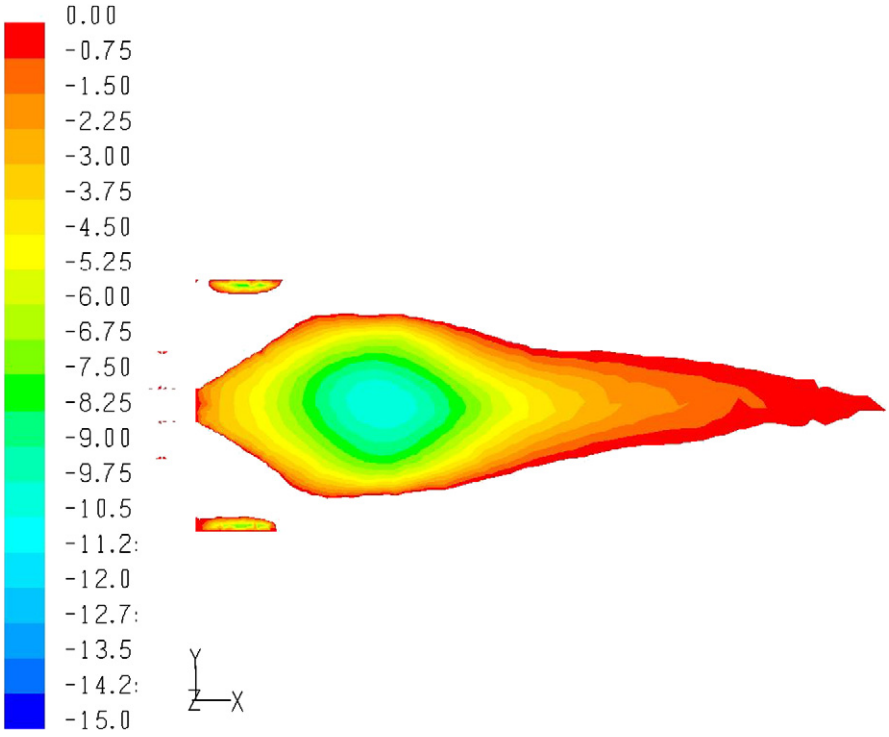

Fig. 32. Velocity contour within the recirculation zone for 8 blades of 45° swirler.

8.3. *Effect of number of vanes*

Having optimized the vane angle, a parametric study has been carried out to examine the effect of number of vanes. For this, the geometry of the 45° vane swirler with 4, 8 and 12 blades with an overlap angle of 30° is selected and the geometries are created in GAMBIT pre-processor and then exported to FLUENT solver. Figs. 31 to 33 show the recirculation zone obtained for 45° swirler with 4, 8 and 12 blades respectively. A larger recirculation zone is obtained for both 8 and 12 vanes

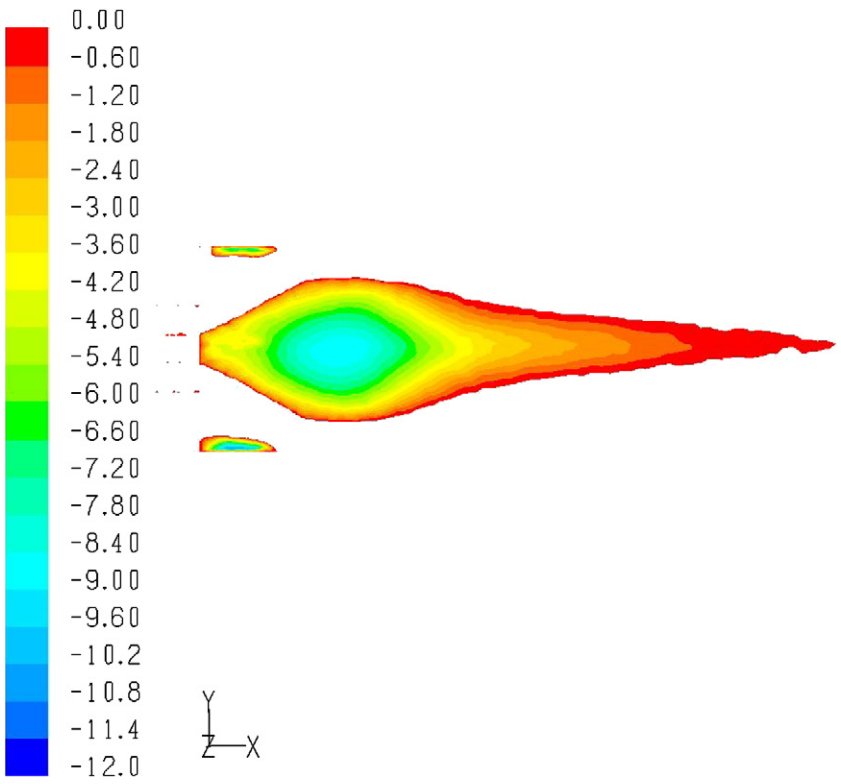

Fig. 33. Velocity contour within the recirculation zone for 12 blades of 45° swirler.

Table 2
Comparison of swirl flow characteristics for varying number of vanes

Number of vanes	Blade length (mm)	Maximum reverse velocity (m/s)	Total pressure drop (Pa)	Turbulent kinetic energy (m^2/s^2)
4	146	−9.47	2110	41.5
8	96	−10.4	1490	47
12	78	−10.1	1560	42.6

whereas comparatively smaller for 4 vanes swirler. The length of the vanes for 45° swirler with 4 vanes is 146 mm and that of 8 vanes and 12 vanes are 96 and 78 mm respectively as given in Table 2. It is seen from Table 2 that the total pressure drop across 4 vanes swirler is 2110 Pa, 1490 Pa for 8 vanes swirler and 1560 Pa for 12 vanes swirler. The total pressure drop across 4 vanes swirler is 29.38% higher than with 8 vanes swirler. This is because the swirler with 4 vanes provides more blockage to the flow because of its length as seen in Fig. 34. The total pressure drop across 12 vanes is 4.48% higher than that of 8 vanes swirler. This is due to the reason that more blockage area to the flow is provided by the increase in number of vanes.

It is found that the turbulent kinetic energy for 8 vanes swirler is 11.70% higher than 4 vanes swirler and 9.36% higher than 12 vanes swirler. Hence, 8 vanes swirler provides better mixing of fuel and air compared with 4 and 12 vanes swirler.

From the present study, it can be concluded that 45° swirler with 8 vanes provides better recirculation characteristics with comparatively lesser pressure drop.

8.4. *Effect of hub*

As a logical extension the effect of hub on swirl flow field characteristics has been studied. For this analysis swirler with hub to tip ratio of 0.3 and a hubless swirler are considered. The design methodology for both the hubless and annular swirlers are same and the details are given in Fig. 35. For the annular swirler, the hub diameter is 32 mm, which corresponds to a hub to tip ratio of 0.3, and for the hubless swirler it is 0. The external diameter in both the cases remains the same at 107 mm. The length of both the hubless and annular swirler also remains the same.

8.4.1. *Axial velocity profiles and recirculation zone*

Figs. 36 and 37 show the axial velocity profiles from stations A to F and G to L respectively for both swirlers. The blue color line indicates the axial velocity profile obtained with hubless swirler and the red color indicates that of for annular swirler.[1] From the figures it can be seen that in case of hubless swirlers the recirculation velocity is slightly higher at immediate downstream of the swirler and this higher negative velocities extends up to 50 mm compared to the annular swirler. This is due to the fact that in case of hubless swirler all the vanes meet at a point in the axis and forms larger blockage.

Practically it is quite difficult to manufacture a hubless swirler. Therefore, in practice there should be a hub with minimum diameter to hold the vanes. In such case, the above difference in recirculation velocity will be almost negligible as

[1] For colors see the web version of this article.

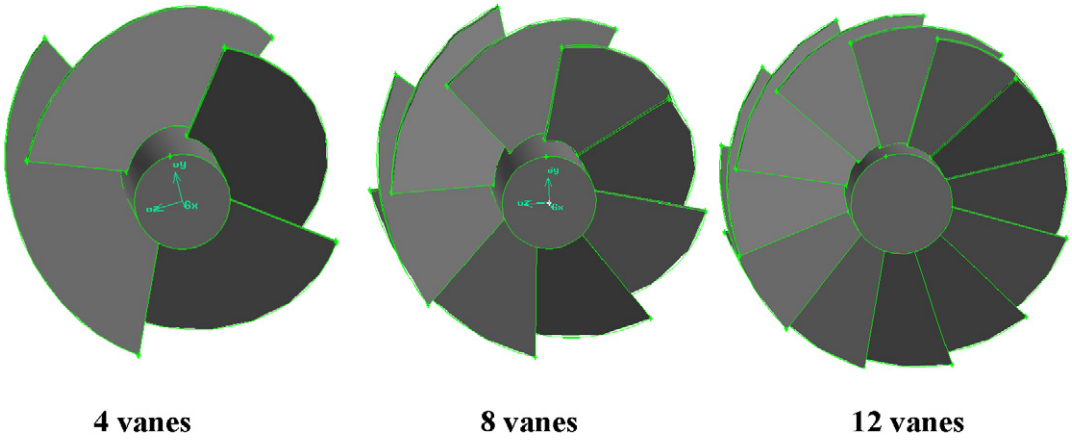

Fig. 34. 45° annular vane swirlers with varying number of vanes.

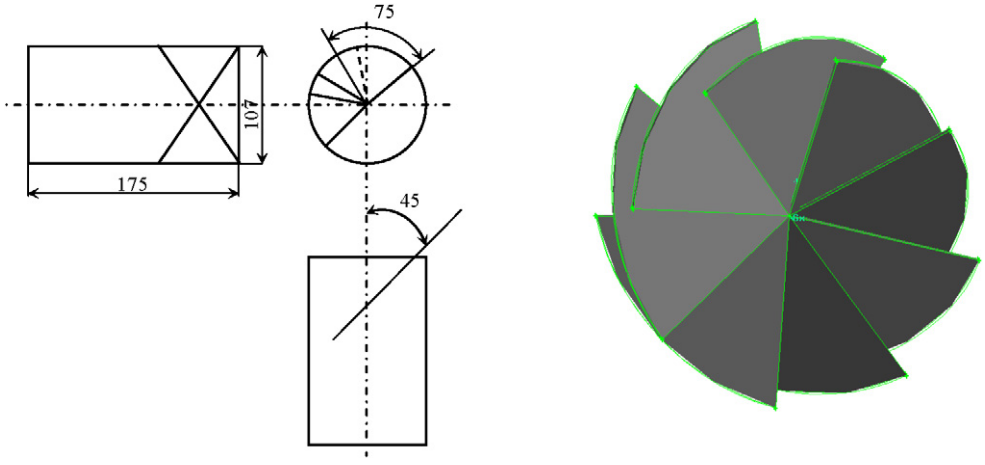

Fig. 35. Design details of 45° hubless swirler.

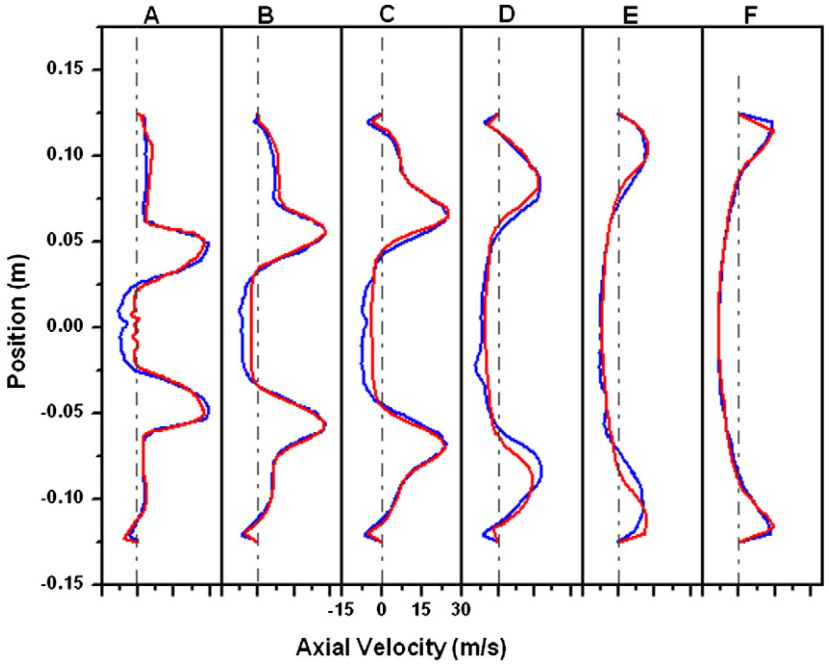

Fig. 36. Comparison of axial velocity contour of 45 vane swirler (A to F).

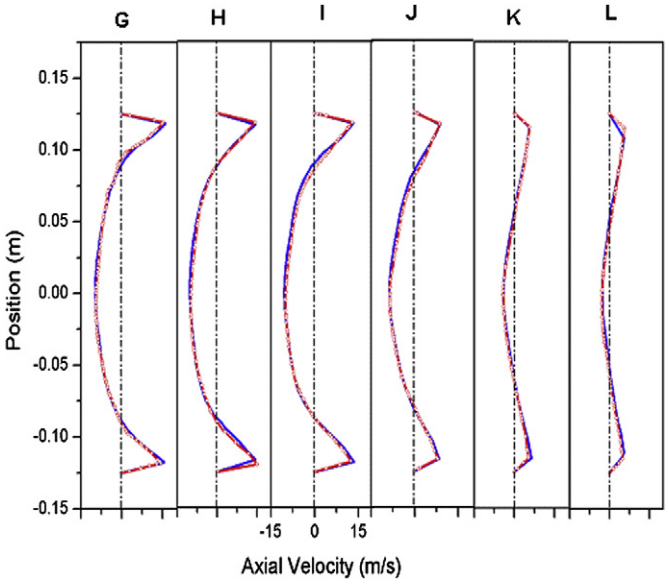

Fig. 37. Comparison of axial velocity contour of 45° vane swirler (G to L).

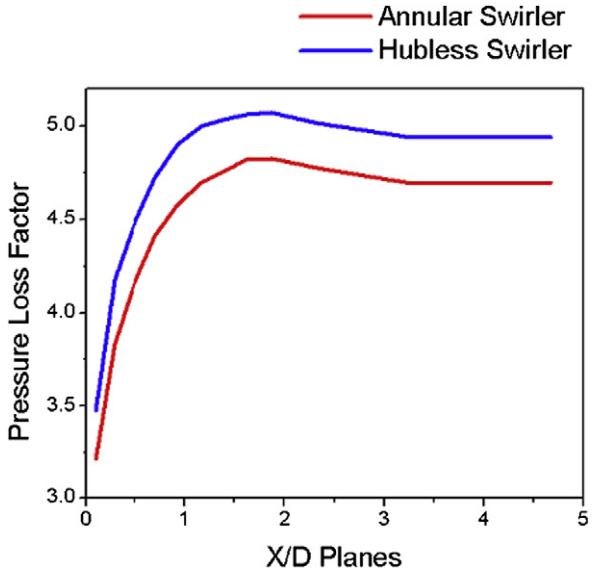

Fig. 38. Pressure loss factor of hubless and annular swirler.

reported in Ref. [12]. The axial velocity profiles from planes E to L are closely matching for hubless and annular swirlers. Thus the effect of hub on flow field characteristics downstream of the swirler is minimal and therefore, it can be ignored considering the practical difficulties in fabricating hubless swirlers. The length and width of the recirculation zone are nearly 5D and 2D, for both hubless and annular swirler, where D is the inner diameter of the inlet pipe. It is also found that the maximum recirculation velocity is 10.4 m/s for both the swirlers.

Fig. 38 shows the pressure loss factor for hubless and annular swirler at various X/D planes downstream of the swirler exit plane. The pressure loss factor curves show a similar trend for both type of swirlers and it is slightly high for hubless swirler immediate downstream of the swirler since the flow is brought to stagnation at the center point on the axis. The pressure loss factor increases up to $X/D = 2.1$ (plane A to I) for both the swirler and thereafter reduces slightly and remains more or less constant thereafter till the exit plane. The recirculation zone width also increases in this plane from A to I. The total pressure loss factor between the inlet and exit for annular swirler is 4.70 and that of hubless swirler is 4.94 and the difference is not much. It is found that the value of M_R/M_O remains almost the same as 0.77 for both the swirlers with almost same total pressure drop. Hence it is seen that the effect of hub with respect to maximum reverse mass flow is also negligible. Hence, it could be concluded from the present study that the effect of hub on swirl flow field characteristics is negligible and the flow field characteristics are the same for both the swirler for the vane angle investigated. Hence, wherever required having a hub will not affect the downstream development of the flow up to a hub to tip ratio of 0.3, as investigated in the present study.

9. Conclusions

1. Standard k–ε model of turbulence predicts the low swirls quite well and RSM predicts well high swirl flows.
2. The 45° vane swirler produces better swirl flow field characteristics, which may aid better mixing of fuel and air for complete combustion.
3. From the parametric study carried out with varying number of vanes, it is found that 45° swirler with 8 number of vanes is the best for producing appropriate recirculation zone.
4. It is found that the swirl flow field characteristics are same for both hubless and annular swirlers investigated. Hence, it is concluded that having a hub with hub to tip ratio of 0.3 will not affect the flow downstream of the swirler.
5. Overall it can be concluded from the aerodynamic studies carried out that a 45° vane swirler with 8 vanes with a hub to tip ratio of 0.3 will be more appropriate for providing good flame stabilization characteristics.

References

[1] M.L. Mathur, N.R.L. Maccallum, Swirling air jets issuing from vane swirlers. Part 1: free jets, Journal of the Institute of Fuel 214 (1967) 214–225.
[2] M.L. Mathur, N.R.L. Maccallum, Swirling air jets issuing from vane swirlers. Part 2: enclosed jets, Journal of the Institute of Fuel 214 (1967) 238–245.
[3] R.F. Huang, F.C. Tsai, Observations of swirling flows behind circular disks, AIAA Journal 39 (2001) 1106–1112.
[4] P.L. Buckley, R.R. Craig, D.L. Davis, K.G. Schwartzkopf, The design and combustion performance of practical swirlers for integral rocket/ramjets, AIAA Journal 21 (5) (1983) 733–740.
[5] N.A. Chigier, J.M. Beer, Velocity and static pressure distribution in swirling air jets issuing from annular and divergent nozzles, Journal of Basic Engineering 4 (1964) 788–796.
[6] S.C. Favaloro, A.S. Nejad, S.A. Ahmed, Experimental and computational investigation of isothermal swirling flow in an axisymmetric dump combustor, Journal of Propulsion 7 (3) (1991) 348–357.
[7] S. Fuji, K. Eguchiand, M. Gomi, Swirling jets with and without combustion, AIAA Journal 19 (11) (1981) 1438–1442.
[8] B.T. Vu, C. Goulding, Flow measurements in a model swirl combustor, AIAA Journal 20 (5) (1982) 642–651.

[9] V. Ganesan, Recirculation and turbulence studies in an isothermal model of a gas turbine combustor chamber, Ph.D. Thesis, I.I.T.-Madras, Chennai, India, 1974.

[10] S.H. Chue, Pressure probes for fluid measurements, Prog. Aero Sciences 16 (1975) 147–223.

[11] D.L. Rhode, D.G. Lilley, D.K. Mclaughlin, Mean flow fields in axisymmetric combustor geometries with swirl, AIAA Journal 21 (1983) 593–600.

[12] S.A. Beltagui, N.R.L. Maccallum, Aerodynamics of vane-swirled flames in furnaces, Journal of the Institute of Fuel 49 (1976) 183–193.